Human Molecular Genetics, 2022, Vol. 31, No. 7 1051–1066

https://doi.org/10.1093/hmg/ddab304
Advance Access Publication Date: 21 October 2021
General Article

GENERAL ARTICLE

C/D box snoRNA SNORD113-6/AF357425 plays a dual role in integrin signalling and arterial fibroblast function via pre-mRNA processing and 2′O-ribose methylation

Eva van Ingen[1,2,‡], Daphne A.L. van den Homberg[1,2,‡], M. Leontien van der Bent[1,2], Hailiang Mei[3], Nikolina Papac-Milicevic[4], Veerle Kremer[6], Reinier A. Boon[6,7,8], Paul H.A. Quax[1,2], Johann Wojta[5,9] and A. Yaël Nossent[1,2,4,5,*,†]

[1]Department of Surgery, Leiden University Medical Center, Leiden, The Netherlands, [2]Einthoven Laboratory for Experimental Vascular Medicine, Leiden University Medical Center, Leiden, The Netherlands, [3]Biomedical Data Sciences, Leiden University Medical Center, Leiden, The Netherlands, [4]Department of Laboratory Medicine, Medical University of Vienna, Vienna, Austria, [5]Department of Internal Medicine II, Medical University of Vienna, Vienna, Austria, [6]Department of Physiology, Amsterdam Cardiovascular Sciences, Vrije Universiteit, Amsterdam UMC location VUMC, Amsterdam, The Netherlands, [7]Institute for Cardiovascular Regeneration, Centre for Molecular Medicine, Goethe University, Frankfurt am Main, Germany, [8] German Center for Cardiovascular Research (DZHK), Frankfurt am Main, Germany and [9] Ludwig Boltzmann Institute for Cardiovascular Research, Vienna, Austria

*To whom correspondence should be addressed at: Medical University of Vienna, Anna Spiegel Forschungsgebäude, 25.2.7.007, Lazarettgasse 14, Vienna 1090, Austria. Email: anne.nossent@meduniwien.ac.at; a.y.nossent@lumc.nl

Abstract

We have previously shown that C/D box small nucleolar RNAs (snoRNAs) transcribed from the DLK1-DIO3 locus on human chromosome 14 (14q32) are associated with cardiovascular disease. DLK1-DIO3 snoRNAs are ‘orphan snoRNAs’ that have no known targets. We aimed to identify RNA targets and elucidate the mechanism-of-action of human SNORD113-6 (AF357425 in mice). As AF357425-knockout cells were non-viable, we induced overexpression or inhibition of AF357425 in primary murine fibroblasts and performed RNA-Seq. We identified several pre-mRNAs with conserved AF357425/SNORD113-6 D′-seed binding sites in the last exon/3′ untranslated region (3′UTR), which directed pre-mRNA processing and splice-variant-specific protein expression. We also pulled down the snoRNA-associated methyltransferase fibrillarin from AF357425-High versus AF357425-Low fibroblast lysates, followed by RNA isolation, ribosomal RNA depletion and RNA-Seq. Identifying mostly mRNAs, we subjected these to PANTHER pathway analysis and observed enrichment for genes in the

[†]A. Yaël Nossent, http://orcid.org/0000-0002-2155-4286
[‡]These authors contributed equally.

Received: June 10, 2021. **Revised:** September 3, 2021. **Accepted:** October 13, 2021

integrin pathway. We confirmed 2′O-ribose methylation in six integrin pathway mRNAs (*MAP2K1*, *ITGB3*, *ITGA7*, *PARVB*, *NTN4* and *FLNB*). Methylation and mRNA expressions were decreased while mRNA degradation was increased under AF357425/SNORD113-6 inhibition in both murine and human primary fibroblasts, but effects on protein expression were more ambiguous. Integrin signalling is crucial for cell–cell and cell–matrix interactions, and correspondingly, we observed altered human primary arterial fibroblast function upon SNORD113-6 inhibition.

Introduction

Small nucleolar RNAs (snoRNAs) are a class of non-coding RNAs that guide modifications of other RNA species, mostly of ribosomal RNAs (rRNAs) (1). Typically, there are two types of snoRNAs, named after conserved sequence motives, namely H/ACA box snoRNAs that guide RNA pseudouridylation (Ψ) and C/D box snoRNAs that guide RNA 2′O-ribose methylation (2′Ome) (1). These modifications are essential for normal rRNA processing and function, and thus for protein synthesis (2). SnoRNAs bind their target RNAs via Watson-Crick base-pairing to their antisense boxes (1). Most C/D box snoRNAs have two C box motifs, C and C′, and two D box motifs, D and D′ (1). The ∼9–20 nucleotides upstream of the D and D′ boxes form the antisense boxes of C/D box snoRNAs (1). In case of canonical C/D box snoRNA function, the snoRNA forms a small nucleolar ribonucleoprotein complex with proteins NHP2L1, NOP56, NOP58 and the methyltransferase fibrillarin (1). Binding of an antisense box to a target rRNA results in 2′Ome of the nucleotide bound to the 5th snoRNA-nucleotide upstream of the D or D′ box (1). Because of the strictly conserved base-pairing, rRNA targets can easily be predicted for approximately half of the known snoRNAs (3). However, for the other half, no rRNA targets have been identified and thus, the function of these ‘orphan’ snoRNAs is still unknown (4).

We have previously shown that a cluster of 41 C/D box snoRNAs, SNORD112, SNORD113 1-9 and SNORD114 1-31, transcribed from the DLK1-DIO3 locus on the long arm of human chromosome 14 (14q32; 12F1 in murine cells) is strongly associated with human cardiovascular disease (5). The 14q32 locus also encodes for two other types of non-coding RNAs, namely two long non-coding RNAs (lncRNAs), MEG3 and MEG8 and 54 microRNAs (6). Both the lncRNAs and microRNAs also play a role in cardiovascular physiology and pathology (7–15); however, genetic analyses showed that the role of the snoRNAs in cardiovascular disease is independent of and stronger than the 14q32 lncRNAs and microRNAs (5). However, all 14q32 snoRNAs are orphan snoRNAs and their targets and mechanisms of action are still unknown (16).

The 14q32 snoRNA locus resembles the Prader-Willi locus, a large snoRNA gene cluster on human chromosome 15q11 (17). Both loci encode two clusters of highly similar C/D box snoRNAs, SNORD113 and SNORD114 on 14q32 and SNORD115 and SNORD116 on 15q11. Both loci are imprinted; however, where all 14q32 non-coding RNAs are transcribed from the maternal allele, the 15q11 snoRNAs are transcribed from the paternal allele (18). The loss of imprinting or mutations and deletions in both loci leads to neuro-developmental disorders, Prader-Willi syndrome for 15q11 and either Temple or Kagami-Ogata syndrome for 14q32 (19). In contrast to the Prader-Willi locus, however, no large deletions in the 14q32 snoRNA cluster have been reported; most mutations affect the upstream lncRNA MEG3 or one of three differentially methylated regions (19). The lack of deletions in the snoRNA cluster hints at its importance for survival.

Besides 2′Ome of rRNAs, several non-canonical functions have been described for both canonical and orphan snoRNAs, including the 15q11 snoRNAs. The orphan SNORD115, for example, has been shown to direct alternative splicing, amongst others of the serotonin receptor *5HT2C* (20–22), where the canonical snoRNA SNORD27 directs alternative splicing of *E2F7*, for example (23). C/D box snoRNAs can also direct processing of the 3′UTR of mRNAs and thereby affect protein expression (24). Although the direction of alternative splicing and 3′-end processing appear to be 2′Ome-independent, it has also been shown that C/D box snoRNAs can induce 2′Ome of mRNAs. For example, the RPL13A-snoRNAs U32A and U51 can guide 2′Ome of the Peroxidasin mRNA, leading to mRNA stabilization and repression of translation, thereby increasing mRNA but decreasing protein levels (25). Besides mRNAs, C/D box snoRNAs may also guide 2′Ome of other non-canonical RNA targets. For example, we showed in 2018 that a 14q32 microRNA, miR-487b is subject to 2′Ome in a fibrillarin-dependent, and thus likely in a C/D box snoRNA-dependent, manner (26). Finally, it has also been shown that certain C/D box snoRNAs may be processed into smaller fragments that bind mRNA 3′UTRs and suppress translation in a microRNA-like fashion (27).

In order to elucidate the mechanisms of action of the 14q32 orphan C/D box snoRNAs, we focused on the murine snoRNA AF357425 and the human snoRNA SNORD113-6. The D′-antisense boxes of these two snoRNAs are fully conserved between the two species, are abundantly expressed in vascular tissue and have been shown to play a role in vascular remodelling and cardiovascular disease (5,28). As the DLK1-DIO3 snoRNAs are expressed predominantly in fibroblasts (3), we used CRISPR/Cas9 in order to knock out AF357425 in murine 3T3 fibroblasts. When this strategy proved unsuccessful as the snoRNA appears essential for cell survival, we used antisense technology in order to knock down or overexpress AF357425 expression in primary murine fibroblasts (PMFs) followed by different RNA-Seq strategies, both with and without prior fibrillarin pulldown and rRNA depletion. Based on the RNA-Seq results, we followed up on multiple targets and mechanisms related to pre-mRNA processing, alternative splicing and RNA stability, in both murine and human fibroblasts.

Here, we describe that AF357425/SNORD113-6 plays a dual role in the regulation of mRNA and protein expression via both pre-mRNA processing/splicing and via 2′Ome of mRNA targets, affecting amongst others, the integrin signalling pathway and primary human arterial fibroblast function.

Results

CRISPR/Cas9 knockout of AF357425

In order to elucidate the function of AF357425/SNORD113-6, we aimed to generate AF357425 knockout fibroblasts. We first transfected 3T3 cells with a single guide RNA, GA-AF357425-1+ (Supplementary Material, Table S2), but all of the surviving clones were wild type. We did observe multiple clones that ceased to proliferate and ultimately rounded up and died after 3–4 divisions, but with only 6–12 cells, we could not analyse these. We then used a combination of four vectors with four different guide RNAs, all aimed to target AF357425, but at different sites

(Supplementary Material, Table S2). We identified 34 single-cell clones, of which nine ceased to proliferate and died after only a few divisions. The remaining 25 clones all showed normal expression of the mature AF357425 snoRNA by RT/qPCR. However, when analysing the genomic DNA PCR product on a 2.5% agarose gel, clone BF6 (plate B, well F6) showed two bands rather than one: the first band (BF6-L) appeared to be similar or slightly longer in length than the wild-type 3T3 band, and the second band (BF6-S) was clearly shorter (Supplementary Material, Fig. S1A). Sanger sequencing of the two alleles showed that the BF6-L allele has a single C-insert directly upstream of the shortest predicted D′-seed, whereas the D′-seed is almost completely deleted by a 9-nucleotide deletion in the BF6-S allele (Supplementary Material, Fig. S1B). Given that AF357425 expression was normal in the BF6, and the cells grow normal and appear in every way similar to wild-type 3T3 fibroblasts, we hypothesized that BF6-L is the maternal and expressed allele.

We then used a novel single guide RNA to knock out the BF6-L allele in the BF6 clone. We observed a ∼99% lethality in the transfected cells, indicating that AF357425 is essential for cell proliferation and ultimately for cell survival.

Inhibition and overexpression of snoRNAs using oligonucleotides

SnoRNA expression was inhibited using gapmers (GM). As shown before, the efficiency of snoRNA inhibition was, however, variable(29) and appeared sensitive to factors including cell cycle, cell density and number of passages (the latter for primary cells only). Even though we controlled for these factors as much as possible, knockdown efficiency was checked for each individual experiment. SnoRNA knockdown was more efficient in primary cells, both human umbilical cord arterial fibroblasts (HUAFs) and PMFs than in human BJ and murine 3T3 and BF6 cells. For primary cells, a knockdown between 60–75% was deemed successful, for cell lines, a knockdown of 20–50% was deemed successful. Cells with less efficient or no knockdown were not used for further experiments or analyses.

Overexpression of the snoRNA AF357425 was achieved using 3rd generation antisense oligonucleotides (3GA) directed towards the 3′-end of the snoRNA. We have shown previously that 3GAs can efficiently induce snoRNA expression, most likely through protection from degradation by endonucleases (5). Representative snoRNA inhibition and overexpression (in PMFs only) per cell line are shown in Supplementary Material, Figure S2.

RNA-Seq of processing/splicing variants

As it was previously reported that snoRNAs can affect RNA processing and RNA stability (24,30,31), we isolated total RNA from the lysates of PMFs transfected with either 3GA-AF357425 (3GA-AF; AF357425-high) or GM-AF357425 (GM-AF; AF357425-low) and sent these to BGI for whole-transcriptome RNA-Seq. The 3GA/GM-induced upregulation/knockdown for this RNA-Seq experiment, as well as the RNA-binding protein immunoprecipitation (RIP)-Seq described later, is shown in Supplementary Material, Figure S2A.

The data from this RNA-Seq experiment were used to identify changes in pre-mRNA processing. After selecting for the presence of a conserved AF357425/SNORD113-6 D′ box seed antisense sequence, we identified 46 genes that showed differential expression of splice- or processing-variants between the AF357425-high and AF357425-low samples. Out of these, four genes had a binding site in the first exon, eight in an internal exon, nine had a binding site in an intron, and 31 genes had a binding site in the last exon, either in the coding sequence or in the 3′UTR (Fig. 1A). We decided to focus on these last exon-binding sites. Of these 31 genes, splice- or processing variants were also conserved in 20 human genes, which further narrowed down our selection (Fig. 1B). In the human genes, we allowed for single-nucleotide mismatches in the D′ box seed antisense sequence, except for nucleotides 4–6 upstream of the D′ box. Although both binding sites and splice- or processing variants were conserved between mice and men, differences were observed in the location, including the 'last exon site', of the predicted snoRNA binding sites between the two species (Supplementary Material, Fig. S3).

The analysed RNA-Seq data are available in Supplementary Material, Excel File 1.

Validation of processing/splicing variants

PANTHER pathway analysis did not point towards pathways that are relevant for cardiovascular disease, so instead, we decided to follow up on three genes, namely *JAG1*, *DUSP7* and *EBPL*, which were abundantly expressed in both murine 3T3 (and BF6) and human BJ fibroblasts. Information on known splice variants was taken from the Ensembl Genome Browser (https://m.ensembl.org/; June 2020; Supplementary Material, Fig. S3). Supplementary Material, Figure S3 also shows details on putative snoRNA binding sites, as well as binding sites for the primer sets that were used. As we chose to focus on the location of the binding site, variants with a binding site in the 3′UTR, or at least in an exon (in that order) were called variant 1. If both variants had similarly located binding sites, the variants that code for proteins were called variant 1. Finally, if both variants coded for a protein, the variant with the highest number of snoRNA binding sites was called variant 1 (Supplementary Material, Fig. S3).

JAG1 contains a single binding site for the D′ box seed of SNORD113-6/AF357425, which is located towards the very end of the coding region towards the end of the last exon of transcript variant 1 (*JAG1-1*), both in the human and in the murine gene. Both in humans and in mice, *JAG1-1*, gives rise to a ∼130 kDa protein. JAG1 transcript variant 2 (JAG1-2) has one snoRNA binding in the last exon in murine cells, and one site in the pre-last exon in human cells. *JAG1-2* is not translated in either mice or humans (Supplementary Material, Fig. S3). Looking at mRNA expression of the two variants, we observed that under snoRNA inhibition, the ratio of mRNA *JAG1-1* over *JAG1-2* increased significantly in murine 3T3 and BF6 cells. We observed a similar trend in human BJ cells ($P = 0.053$) (Fig. 2A–C).

DUSP7 has two transcript variants in both mice and humans that both give rise to a protein. In mice, variant 1, *DUSP7-1*, has a snoRNA binding site located in the 3′UTR and gives rise to a ∼40–45 kDa protein. *DUSP7-2* gives rise to a ∼24 kDa protein, but has no binding site for the D′-seed of AF357425. In humans, *DUSP7-1* has a binding site in the 3′UTR and gives rise to a ∼30 kDa protein, whereas *DUSP7-2* has a binding site in the last intron of its pre-mRNA and gives rise to a ∼40–45 kDa protein (Supplementary Material, Fig. S3). Looking at mRNA expression of the two variants, we observed that under snoRNA inhibition, the ratio of mRNA *DUSP7-1* over *DUSP7-2* decreases significantly in murine 3T3 cells, but we observed the opposite in human BJ cells (Fig. 2D–F).

EBPL has two splice variants in both mice and humans. In mice, *EBPL-1* gives rise to a ∼23 kDa protein and has a binding site for the D′-seed of AF357425 in its 3′UTR. *EBPL-2* has no

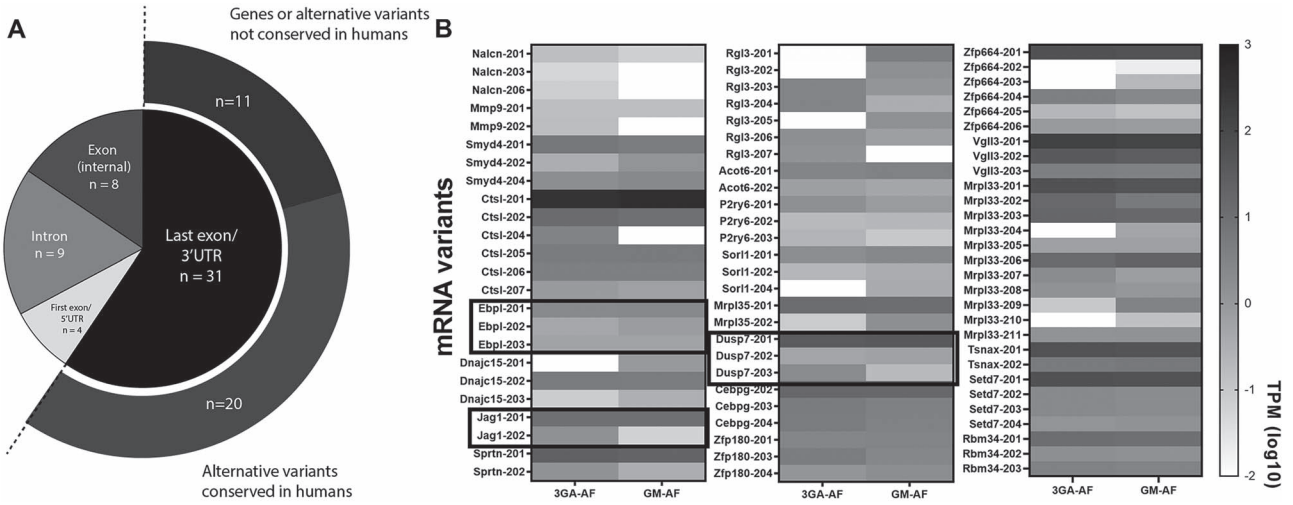

Figure 1. RNA-Seq. (**A**) Schematic representation of genes with multiple splice/processing variants that are differentially expressed between AF357425-High and AF357425-Low sample pool. Conservation between mice and humans is given for variants with D′ box seed binding sites in the last exon/3′UTR of the dominant variant. (**B**) Heatmap of expression changes in variant expression in AF357425-High (3GA-AF) and AF357425-Low (GM-AF) sample pools of genes with conserved D′ box seed binding sites in their last exon/3′UTR.

binding site, nor does it give rise to a protein. In humans, both *EBPL-1* and *EBPL-2* give rise to proteins, ~23 and ~16 kDA, respectively, but *EBPL-1* has more binding sites for the D′-seed of SNORD113-6 (Supplementary Material, Fig. S3). Looking at mRNA expression of the two variants, we observed that under snoRNA inhibition, the ratio of mRNA *EBPL-1* over *EBPL-2* shows a trend towards an increase in murine BF6 cells ($P = 0.064$), and a significant increase in human BJ cells (Fig. 2G–I).

Finally, although we identified them as potential 2′Ome targets via RIP-Seq (described later), *ITGB3*, *PARVB* and *MAP2K1* also have different processing variants in human cells combined with snoRNA binding sites towards the 3′-end of the gene (Supplementary Material, Fig. S3). The *ITGB3-1* pre-mRNA has a binding site for the D′-seed of SNORD113-6 in the last intron, whereas the *ITGB3-2* pre-mRNA lacks this intron and is marked for nonsense-mediated decay (NMD; Ensembl). The inhibition of SNORD113-6 in HUAFs led to a trend towards a decreased ratio of the *ITGB3-1* mRNA over the *ITGB3-2* mRNA ($P = 0.07$; Fig. 2J). For MAP2K1, there are two variants that both have snoRNA binding sites in their introns, but MAP2K1-1 has more sites (12 sites) than the shorter MAP2K-2 (6 sites) and under snoRNA inhibition again the ratio of MAP2K1-1 over MAP2K-2 appeared decreased ($P = 0.068$; Fig. 2K). Finally, the human *PARVB-1* mRNA has a binding site in its 3′UTR, where *PARVB-2* has no binding site. However, here, we did not observe changes in the ratio between the two variants (Fig. 2L).

Overall, it appears as if snoRNA binding in the last exon and 3′UTR, but not in introns, affects pre-mRNA processing and possibly protects the (pre-)mRNA for degradation.

RIP-Seq and pathway analysis

As fibrillarin is the main C/D box snoRNA-associated methyltransferase (1), we also performed a fibrillarin pulldown followed by total RNA isolation on the lysates of AF357425-high and AF357425-low murine fibroblasts in order to identify novel RNA targets that are subject to AF357425-induced 2′Ome. Using both AF357425 overexpression and inhibition (Supplementary Material, Fig. S2A), we aimed to create the largest possible difference between cell pools, hypothesizing that transcripts enriched in the AF357425-high pool are potential 2′Ome targets of AF357425. Samples from multiple transfections and pulldowns had to be pooled to obtain enough RNA for further analysis. Pooled RNA from AF257425-high or AF357425-low was sent to BGI for rRNA depletion followed by RNA-Seq. In total, we detected transcripts from 18.997 genes in the AF357425-High pool and 24.678 genes in the AF357425-Low pool. Within these genes, we selected all those with a conserved, nine-nucleotide antisense sequence for the AF357425 D′ box seed sequence in the coding region and 3′UTR, which were enriched in the AF357425-High pool (407 genes). One mismatch in any position, except for nucleotides 4–6 upstream of the AF357425 D′ box, was allowed. When conserved, these murine genes were converted to human genes (292 genes) and again all genes with a conserved antisense sequence of the SNORD113-6 D′ box, now also in introns, were selected. A perfect antisense sequence was found in 161 genes. Allowing for one mismatch, except for nucleotides 4–6 upstream of the SNORD113-6 D′ box, resulted in additional 67 genes. We used these 228 genes in a PANTHER pathway analyses and found potential enrichment of multiple pathways (Supplementary Material, Excel File 4), of which one, the integrin signalling pathway, stood out, with 7 out of 46 genes in the pathway enriched in the AF357425-high sample pool. Because of its importance in fibroblast function (32), we decided to follow up on the integrin signalling pathway target genes.

The analysed RIP-Seq data are available in Supplementary Material, Excel File 2. An overview of the number of genes and pathways identified is shown in Figure 3.

Validation of 2′Ome targets

We identified seven genes in the integrin signalling pathway as potential conserved fibrillarin-dependent targets for AF357425/SNORD113-6, namely *MAP2K1*, *ITGB3*, *ITGA7*, *FLNB*, *NTN4*, *PARVB* and *COL4A4*. In the murine *Itgb3*, *Flnb*, *Parvb* and *Col4a4* predicted binding sites were all located in the 3′UTR. Binding sites in *Map2k1*, *Itga7* and *Ntn4* were all located in exons. In the human *FLNB* and *PARVB*, binding sites were located in the 3′UTR. Binding sites in human *ITGB3* and *NTN4* were located in the last intron and in *ITGA7* in the last exon. Human *MAP2K1*

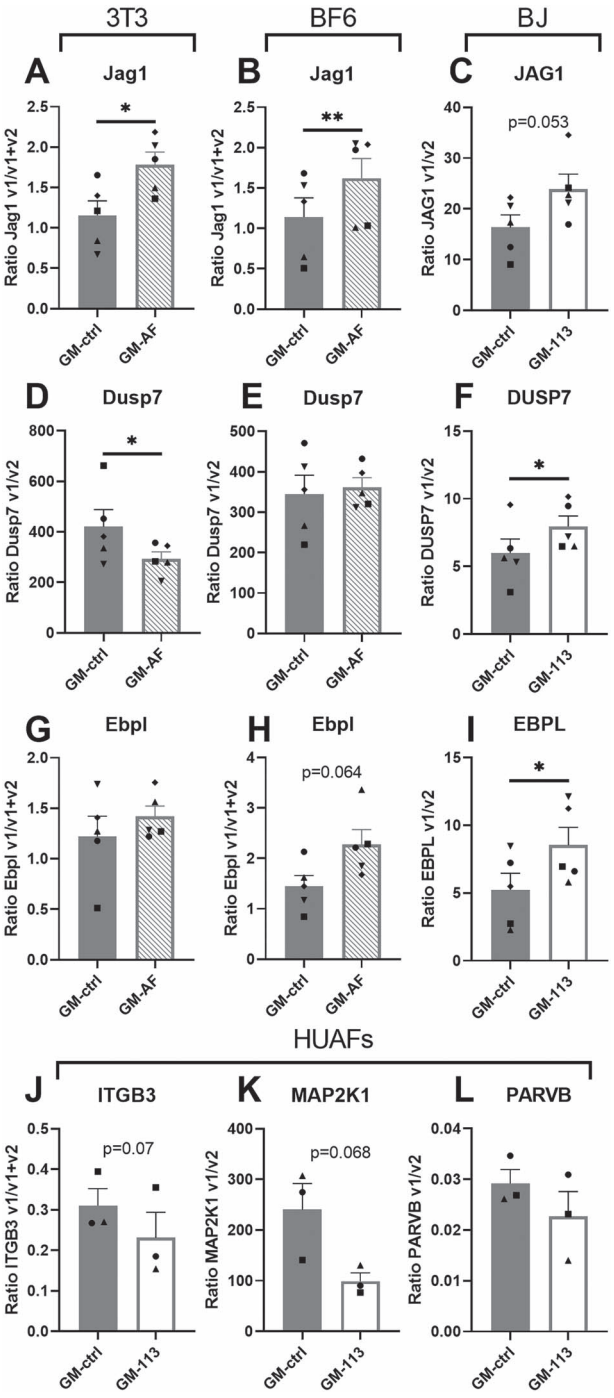

Figure 2. Ratios of splice and processing variants with and without SNORD113-6/AF357425 binding sites. (**A–I**) Ratios of mRNA variants in murine 3T3 and BF6 and in human BJ fibroblasts and (**J–L**) in HUAFs. Variant 1 was measured specifically, but depending on the primer binding sites (Supplementary Material, Fig. S3), we either measured variant 2 alone, or in combination with variant 1, as depicted on the y-axes. Expression levels are relative to GAPDH. A two-tailed paired *t*-test was performed to compare single treatment with the control, within each individual experiment. Data are represented as mean ± SEM. $^*P < 0.05$, compared with GM-ctrl.

and *COL4A4* had multiple predicted binding sites, 12 and 3, respectively, all located in introns. Binding site locations are indicated with an * in Supplementary Material, Figure S3, those sites at which 2′Ome was measured are indicated with the full binding site sequence.

We performed Reverse Transcription at Low dNTP concentration followed by Quantitative (RTL-Q) PCR (26) in order to confirm and quantify methylation at the predicted site in both the murine and human genes in primary fibroblasts (PMFs and HUAFs, respectively). We indeed found 2′Ome in both the murine and human *MAP2K1*, *ITGA7* and *NTN4* mRNA (Fig. 4B–D, G, I and K). We also found 2′Ome at the predicted site of the murine *Itgb3* mRNA (Fig. 4A), as well as in the human *PARVB* and *FLNB* mRNA (Fig. 4H and J). We then calculated the 'estimated methylated fraction' (EMF) for each of these sites. Although the EMF is an unprecise measure, an estimation by definition, we observed a trend towards reduction of the EMF upon inhibition of either AF357425 or SNORD113-6 for *Itgb3*, *Map2k1* and *Ntn4*, and in PMFs (Fig. 4A, B and D) and for pre-*MAP2K1* in HUAFs (Fig. 4G), indicating that the snoRNA indeed guides 2′Ome at these sites, but that a 60–80% snoRNA knockdown is not nearly enough to abolish all methylation at these sites.

In the remaining identified putative targets, *Col4a4*, *Flnb* and *Parvb* in PMFs and *COL4A4* and *pre-ITGB3* in HUAFs, expression was too low to confirm 2′Ome.

Although both RNA-Seq strategies provide different sorts of information, i.e. altered expression of different transcript versus snoRNA-induced binding to fibrillarin, both strategies provided us with potential AF357425 targets. Therefore, besides the integrin signalling pathway genes alone, we also measured potential 2′Ome in the AF357425 targets that were identified through the splicing/processing route described earlier. We confirmed 2′Ome at the predicted sites in the murine and human *DUSP7* mRNA (Fig. 4F and L), in the murine *Jag1* mRNA (Fig. 4E) and in the human *EBPL* mRNA (Fig. 4M). In HUAFs, *JAG1* and in PMFs *Ebpl* expression were too low to quantify potential 2′Ome.

Effects of 2′Ome on mRNA stability

It has been postulated that 2′Ome can stabilize RNAs and thereby reduce RNA degradation rates (30,31). Therefore, after a 24-hour transfection with GMs, we treated HUAFs and PMFs with the transcription inhibitor Actinomycin D and measured mRNA levels after 2 and 6 h, in order to determine the rate of mRNA degradation after snoRNA inhibition and decreased (pre-)mRNA 2′Ome. We used the same primer sets used to measure the EMF (earlier); however, we also measured mRNA degradation using the splice variant-specific primers sets (data shown in Supplementary Material, Fig. S4).

In murine cells, we confirmed 2′Ome in the *Itgb3*, *Map2k1*, *Itga7*, *Ntn4*, *Jag1 and Dusp7* mRNAs. Additionally, we observed that after transfection with GM-AF357425, total 2′Ome-mRNA was reduced for *Itgb3*, *Map2k1*, *Ntn4* and *Jag1*, compared with GM-Ctrl. In accordance, the *Itgb3* mRNA showed a trend towards increased degradation upon snoRNA inhibition ($P = 0.081$; Fig. 5A). *Map2k1*, *ItgA7*, *Ntn4* and *Jag1* showed similar trends ($P = 0.079$, $P = 0.113$, $P = 0.75$ and $P = 0.130$, respectively; Fig. 5B–E), whereas degradation of the *Dusp7* mRNA was increased significantly ($P = 0.005$; Fig. 5F).

In human cells, we confirmed 2′Ome in the *pre-MAP2K1*, *PARVB*, *ITGA7*, *FLNB*, *pre-NTN4*, *DUSP7* and *pre-EBPL* (pre-)mRNAs. Moreover, we found that after transfection with GM-SNORD113-6, total 2′Ome-mRNA was reduced for *pre-MAP2K1*, *DUSP7* and *EBPL*, compared with GM control (GM-ctrl). In accordance, degradation of the *pre-MAP2K1*, *PARVB*, *ITGA7*, *pre-NTN4*, *DUSP7* and *pre-EBPL* (pre-)mRNAs was increased significantly (Fig. 5G–M).

As discussed earlier, *DUSP7*, *JAG1* and *EBPL* have transcript variants with and without AF357425/SNORD113-6 binding sites.

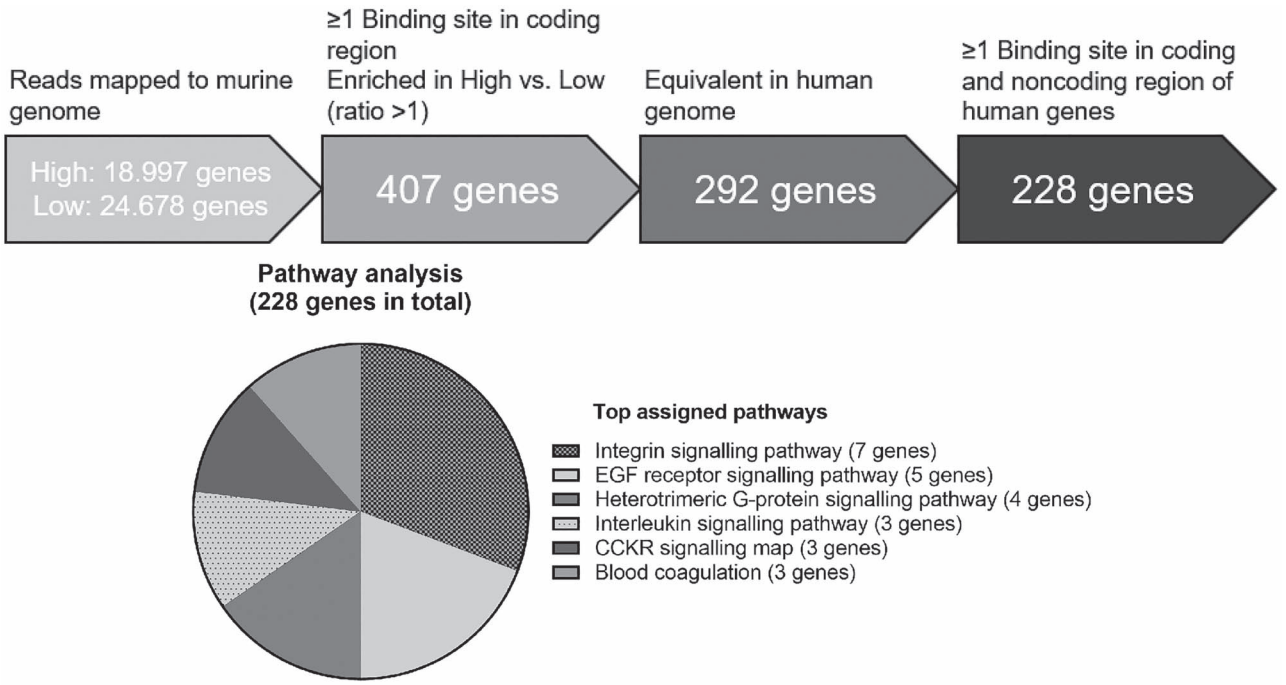

Figure 3. RIP-Seq and pathway analysis. Schematic representation for genes selected from the RIP-seq. RNA-seq was performed on RNA from pooled fibrillarin pulldowns of AF357425-High (3GA-AF) and AF357425-Low (GM-AF) treated PMFs. One mismatch in any position of the nine-nucleotide antisense sequence for the AF357425 D′ box, except for nucleotides 4-6 upstream of the AF357425 D′ box, was allowed. Similar criteria were used for SNORD113-6 binding sites in human genes. Pathway enrichment analysis was performed on the remaining set of potential target genes using PANTHER Classification System.

Human *MAP2K1* has two splice variants, which contain 12 and 6 intronic 2′Ome sites, respectively (Supplementary Material, Fig. S3). In human *MAP2K1, JAG1 and DUSP7* snoRNA inhibition resulted in, a trend or significant, increased degradation of the one variant, but not the other (Supplementary Material, Fig. S4I, J, and M–P), confirming previous studies that showed that 2′Ome protects (pre-)mRNAs from degradation (25). In mice, we observed the same effect for Jag1-2 and Dusp7-1 (Supplementary Material, Fig. S4A–D).

Protein expression

Based on our findings on (pre-)mRNA processing/splicing, 2′Ome, mRNA-stability and the availability of reliable antibodies, we used Western blotting to study the effects of AF357425/SNORD113-6 knockdown in primary human and murine fibroblasts on protein expression of JAG1, DUSP7, ITGB3 and MAP2K1 (Fig. 6A and B).

Although we observed effects of snoRNA knockdown on pre-mRNA processing in both human and murine cells, and on methylation and mRNA degradation in murine cells, there was no effect on protein expression of JAG1 in either murine or human fibroblasts (Fig. 6C and D). DUSP7 protein expression was also unaffected in murine primary fibroblasts (Fig. 6E), but in human primary fibroblast, protein expression of DUSP7-2 (~40 kDa, Fig. 6B) was upregulated under SNORD113-6 inhibition ($P = 0.052$; Fig. 6F), whereas DUSP7-1 (~30 kDa) was not detected by western blot. This is in conflict with the decrease in mRNA stability of *DUSP7-2* under snoRNA inhibition (Supplementary Material, Fig. S4P).

In murine cells, ITGB3 also showed a trend towards increased protein expression, whereas in human cells, ITGB3 protein expression was significantly reduced under snoRNA inhibition (Fig. 6G and H). Like the human *(pre-)DUSP7*, the murine *Itgb3* mRNA is methylated and methylation is reduced under snoRNA inhibition. It has been shown previously that mRNA methylation can inhibit translation (25), which may explain the increased protein expression under snoRNA inhibition, an effect that is not seen for the unmethylated human *ITGB3*. In human cells, *ITGB3* was not methylated, but has at least two processing variants. Under snoRNA inhibition, we found that the mRNA ratio changes in favour of *ITGB3-2*, which is marked for NMD (Ensembl). This is confirmed by a decreased protein expression in HUAFs under SNORD113-6 inhibition.

Finally, we looked at protein expression of MAP2K1. MAP2K1 protein expression was significantly downregulated in murine fibroblasts under inhibition of AF357425 (Fig. 6I). This is in accordance with the increased mRNA degradation; however, it conflicts with notion that 2′Ome inhibits translation. The 2′Ome of the murine *Map2k1* mRNA is located in the coding region, whereas 2′Ome in *Itgb3* is located in the 3′UTR. Whether, and if so, how much, the location of 2′Ome affects translation remains to be determined. In contrast to murine fibroblasts, MAP2K1 protein expression showed a trend towards upregulation in human fibroblasts under SNORD113-6 inhibition ($P = 0.061$; Fig. 6J). However, in human cells, MAP2K1 has two splice variants that give rise to a protein. We were able to detect and quantify both variants. When we calculated the ratio MAP2K1-1:MAP2K1-2, this ratio was significantly increased under snoRNA inhibition, which is in accordance to the change in mRNA ratios (Fig. 6L). The human *MAP2K1-1* pre-mRNA only has intronic 2′Ome sites, which would not impact translation.

Effects of integrin pathway 2′Ome on fibroblast function

Clearly, the effects of AF357425/SNORD113-6 on protein expression of its target (pre-)mRNAs is complex and depends on amongst others the location of the binding site and whether

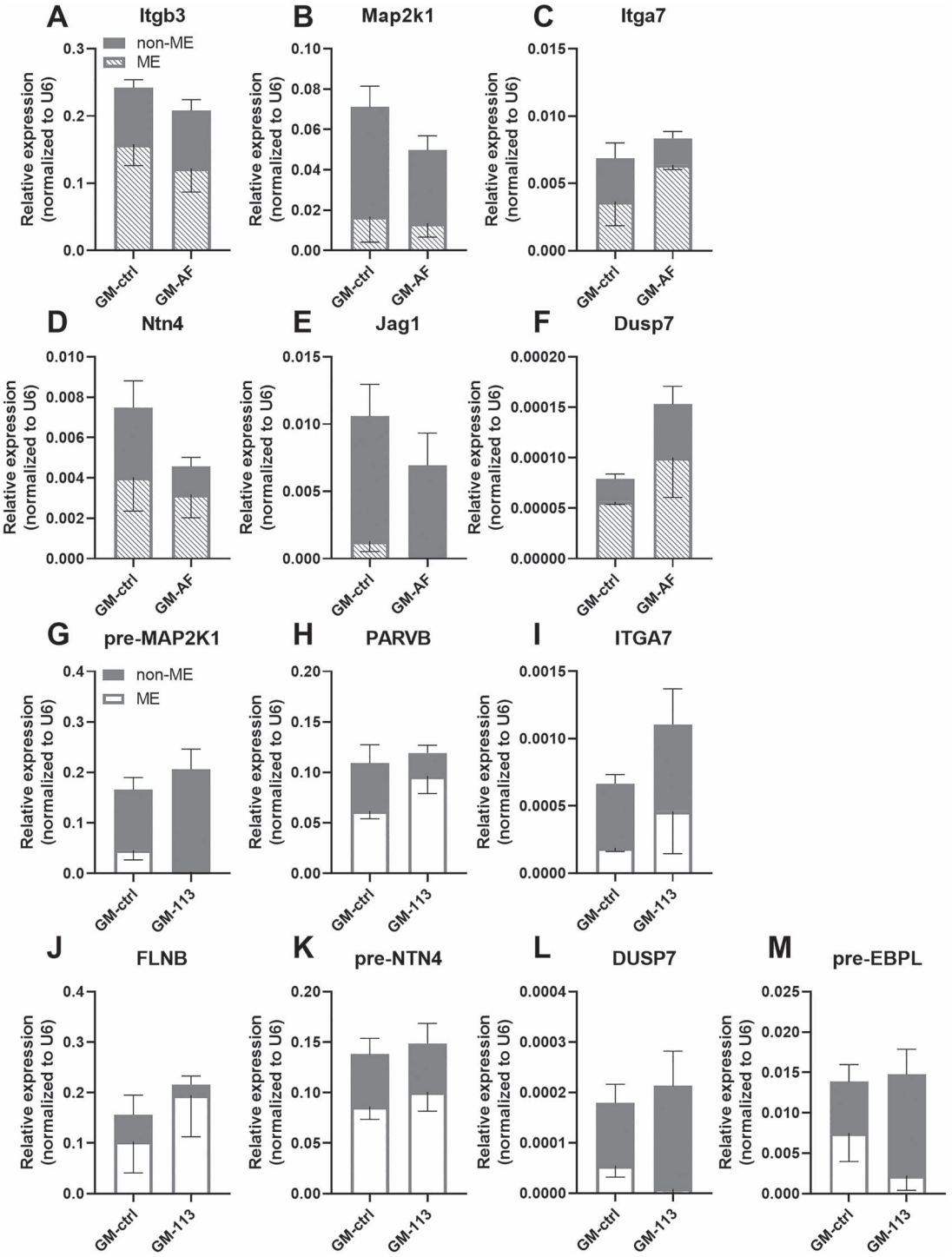

Figure 4. 2′-O-methylation at predicted SNORD113-6/AF357425 binding sites. For the detection of 2′-O-methyated nucleotides, RTL-Q was performed. PMFs or HUAFs were transfected with GM-ctrl or GMs against murine AF357425 (GM-AF) or human SNORD113-6 (GM-113) for 24 h. The EMF was calculated and shown as part of the relative gene expression. Relative expression and EMF of murine targets (**A**) *Itgb3*, (**B**) *Map2k1*, (**C**) *Itga7*, (**D**) *Ntn4*, (**E**) *Jag1* and (**F**) *Dusp7* in PMFs transfected with GM-ctrl or GM-AF. Relative expression and EMF of human targets (**G**) pre-*MAP2K1*, (**H**) *PARVB*, (**I**) *ITGA7*, (**J**) *FLNB*, (**K**) pre-*NTN4*, (**L**) *DUSP7* and (**M**) *pre-EBPL* in HUAFs transfected with GM-ctrl or GM-113. Expression levels are relative to U6. Data are represented as mean ± SEM.

binding leads to 2′Ome or not. Therefore, we aimed to look at effects of SNORD113-6 inhibition on fibroblast function, rather than merely on protein expression. Integrin signalling is an essential pathway in fibroblasts, affecting fibroblast interaction both with other fibroblasts and with the extracellular matrix (32). We analysed the barrier function of HUAFs that were seeded in a monolayer. After seeding, there is a rapid peak in barrier function, which is caused by the initial adherence of the cells. This peak appears somewhat earlier and higher in GM-ctrl transfected HUAFs than in GM-113 transfected HUAFs, indicating

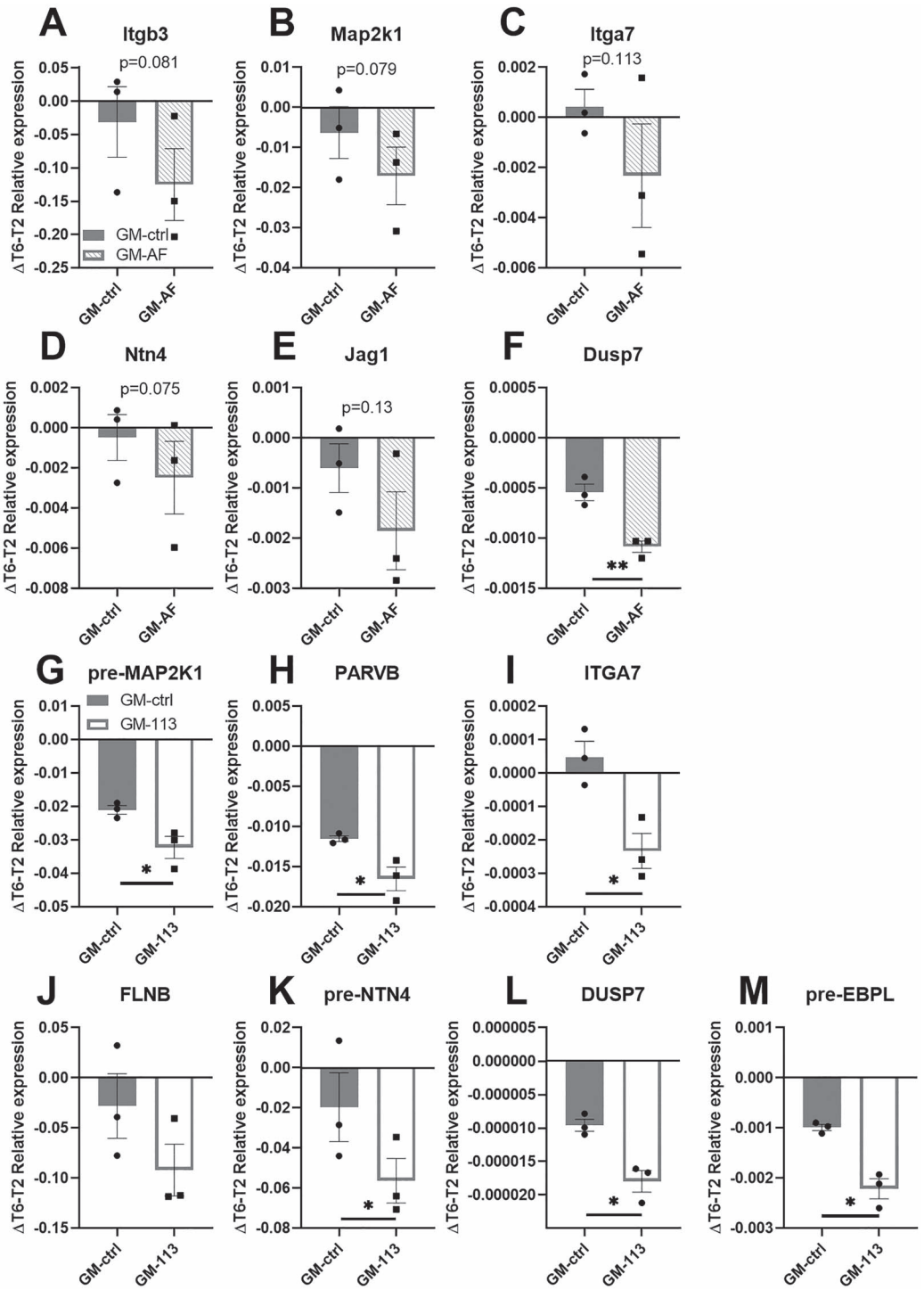

Figure 5. Stability of SNORD113-6/AF357425 target mRNAs in primary cells. PMFs or HUAFs were transfected with GM-ctrl or GMs against murine AF357425 (GM-AF) or human SNORD113-6 (GM-113) for 24 h. After 24 h, cells were treated with Actinomycin D to inhibit novel RNA transcription. mRNA levels of SNORD113-6/AF357425 targets were measured 2 (T2) and 6 (T6) h after addition of Actinomycin D. The decline in mRNA was calculated over time as relative expression of T6 minus relative expression of T2 (ΔT6-T2). The decline in mRNA of murine targets (**A**) *Itgb3*, (**B**) *Map2k1*, (**C**) *Itga7*, (**D**) *Ntn4*, (**E**) *Jag1* and (**F**) *Dusp7* in PMFs transfected with GM-ctrl or GM-AF. The decline in mRNA of human targets (**G**) pre-*MAP2K1*, (**H**) *PARVB*, (**I**) *ITGA7*, (**J**) *FLNB*, (**K**) pre-*NTN4*, (**L**) *DUSP7* and (**M**) *pre-EBPL* in HUAFs transfected with GM-ctrl or GM-113.6. A one-tailed paired *t*-test was performed to compare increased decline in GM-AF/113 compared with GM-ctrl, within each individual experiment. Data are represented as mean ± SEM. $^{*}P < 0.05$, compared with GM-ctrl.

that initial adherence is somewhat impaired under snoRNA inhibition. Over time, however, barrier function of HUAFs is maintained for longer at a higher level under SNORD113-6 inhibition, compared with the negative control (Fig. 7A). There is a trend towards an increased barrier function after 24 h, and a significant increase after 48 h (Fig. 7B and C). It should be noted that we cannot fully exclude effects of potential changes in cell proliferation rates between GM-113 and GM-ctrl treated cells.

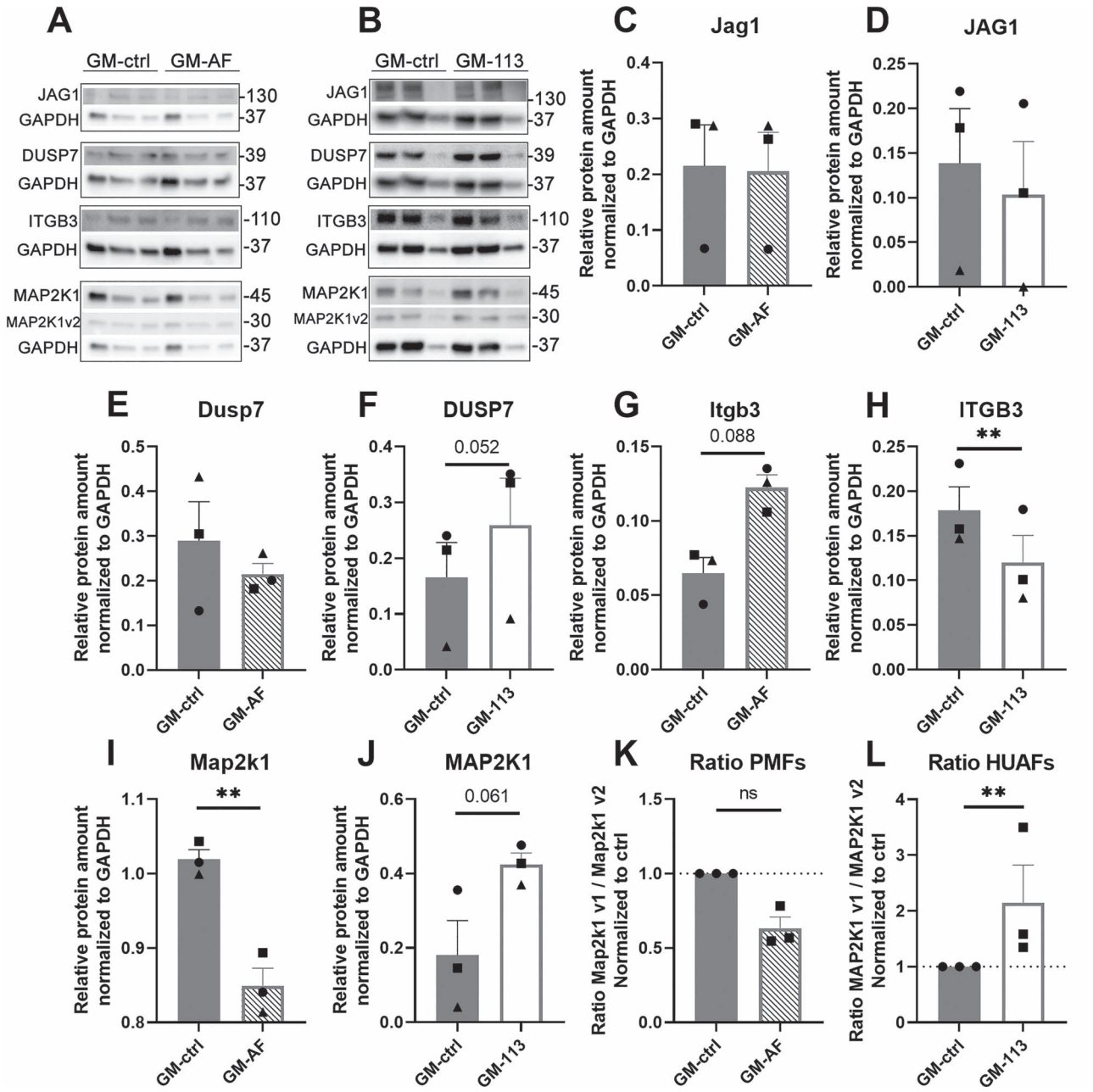

Figure 6. Protein expression in murine and human primary fibroblasts. (**A**) Western blots for JAG1, DUSP7, ITGB3 and MAP2K1, each with GAPDH, of three independent replicates (each band represents a pool of three technical triplicates) in PMFs. (**B**) Western blots for JAG1, DUSP7, ITGB3 and MAP2K1, with GAPDH of three independent replicates (each band represents a pool of three technical triplicates) in HUAFs. (**C–L**) Quantifications of protein band intensities, normalized to GAPDH. Data are represented as mean ± SEM. $^{**}P < 0.01$, compared with GM-ctrl.

Therefore, we also assessed the effects of SNORD113-6 inhibition in a collagen contraction assay. Transfected fibroblasts were embedded in 2 mg/ml collagen gels, which were allowed to float in culture medium. The extend of gel contraction was assessed after 24 and 48 h. Already after 24 h, we observed a 9% increase in gel contraction in cells treated with GM-113 compared with GM-ctrl ($P = 0.02$; Fig. 7D). After 48 h we still observed a 6% increase in contraction ($P = 0.075$; Fig. 7E) Finally, we also assessed migratory properties of fibroblasts transfected with GM-113, using a scratch wound healing assay. After 24 h, we observed a 16% increase in wound closure compared with GM-ctrl ($P = 0.01$; Fig. 7F).

Discussion

Because of their previously found association with cardiovascular disease (28), we aimed to identify targets for the orphan DLK1-DIO3 C/D box snoRNAs. We focused on the one of the most abundantly expressed snoRNAs from this locus with a fully conserved (D′ box) seed in mice and humans, AF357425/SNORD113-6 (28). There are no known rRNA targets for this snoRNA (3), but here we show that AF357425/SNORD113-6 can target mRNAs and affects their expression via at least two different mechanisms. We confirm previous studies that showed that snoRNAs direct 3′end processing and splicing of pre-mRNAs (23,24). Our data further

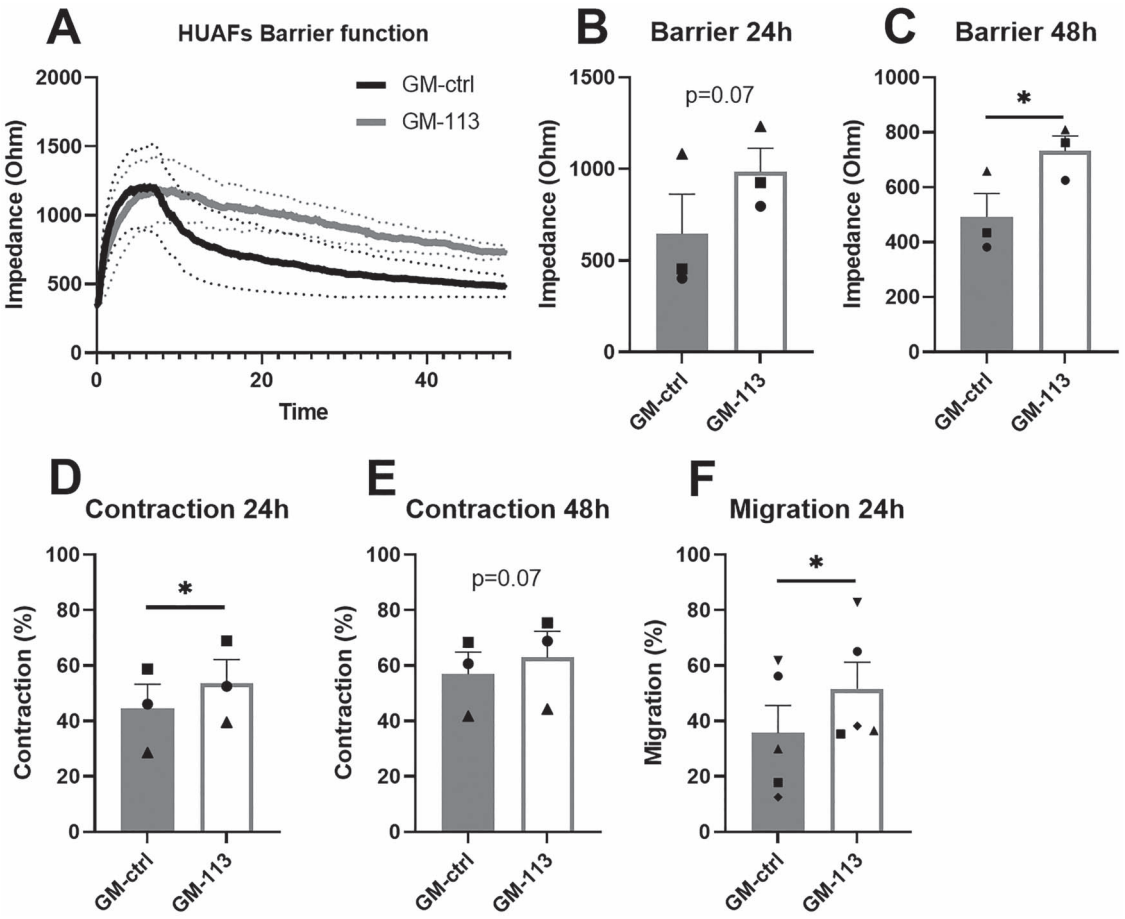

Figure 7. Primary human fibroblast function after SNORD113.6 inhibition. Human arterial umbilical fibroblasts (HUAFs) transfected with GMs against SNORD113.6 (GM-113) or GM-ctrl were plated in electrode plates for ECIS. Impedance (in Ohm) was measured over time for 50 h in total. (**A**) HUAFs barrier function over time in GM-ctrl or GM-113 treated cells. (**B**) Impedance (in Ohm) at 24 h and (**C**) 48 h of incubation. HUAFs transfected with GM-113 or GM-ctrl were mixed into 2 mg/ml collagen gel cushion and cell-induced gel contraction was assessed. (**D**) Percentage of collagen gel contraction at 24 and (**E**) 48 h of incubation. (**F**) HUAFs transfected with GM-113 or GM-ctrl were seeded and subsequently a cross-sectional scratch wound was introduced and scratch wound closure (%) was assessed after 24 h and quantified. A two-tailed paired *t*-test was performed to compare single treatment with the control, within each individual experiment. Data are represented as mean ± SEM. $^{*}P < 0.05$, compared with GM-ctrl.

indicate that AF357425/SNORD113-6 directs fibrillarin towards specific mRNA targets to guide 2′Ome, which may lead to stabilization of the methylated (pre-)mRNA. The latter mechanism, 2′Ome appears better conserved between mice and humans than the pre-mRNA processing. Effects on protein expression; however, were ambiguous and therefore we analysed the effects of SNORD113-6 on cell function in primary human fibroblasts and show that SNORD113-6 regulates cell–cell and cell–matrix interactions as well as cell migration, which is crucial for normal fibroblast function.

As it can be challenging to reliably knock down snoRNAs using antisense oligonucleotides (29), we aimed initially to knock out the murine AF357425 in fibroblasts, using the easy-to-culture and easy-to-transfect NIH-3T3 fibroblast cell line. This strategy proved to be even more challenging than antisense knockdown, as we did not manage to obtain any surviving AF357425-knockout clones. We did, however, frequently observe clones that appeared normal for several divisions, but then stopped to divide, rounded up and ultimately died. Without surviving clones, we cannot prove that the dying clones were indeed knockouts for AF357425, it could simply be that our CRISPR/Cas9 strategy was not successful. However, it has been shown before that other snoRNAs can be knocked out effectively using CRISPR (33). Furthermore, by looking at OFP expression, we found that the Cas9/sgRNA vector was transfected effectively every time. Finally, we did obtain a mutant clone, BF6, which proves that as long as expression and function are not severely affected, the AF357425 gene can be mutated using CRISPR/Cas9. We included the BF6 clone in our further analyses to see if under further snoRNA inhibition, the heterozygous knockout would make these cells behave differently. Imprinting of the locus appeared to be complete, however, even under snoRNA inhibition, as the BF6 behaved very similar to the wild-type 3T3 fibroblasts. Together our findings implicate that AF357425 may be essential for cell survival.

Tightly controlling for cell number, confluency and cell cycle synchronization using KN-93 (34) [serum starvation induces DLK1-DIO3 non-coding RNA expression (35)], we managed to reproducibly induce and inhibit AF357425/SNORD113-6 expression using oligonucleotides. We performed RNA-Seq on AF357425-High versus AF357425-Low samples and found that there was an overrepresentation of (pre-)mRNAs with a snoRNA binding site in the last exon, particularly in the 3′UTR. It has been shown previously that snoRNAs can impact 3′end processing of pre-mRNAs (24) and we could confirm this finding for the AF357425-targets *Jag1*, *Dusp7* and *Ebpl*. However, although we

checked for conservation of the SNORD113-6 binding sites in the human genes, these binding sites were not always located in the last exon. We therefore also confirmed a clear impact of snoRNA binding on the preference for specific splice variants, including for *EBPL* and *MAP2K1*, as has also been shown previously for other orphan snoRNAs (20–23).

Canonical C/D box snoRNAs act as guide RNAs for the methyltransferase fibrillarin to its rRNA targets (1). Although the DLK1-DIO3 snoRNAs have no known rRNA targets, we have shown previously that they do associate with fibrillarin (5), indicating that they guide canonical 2′Ome of non-canonical target RNAs. Here we found that AF357425/SNORD113-6 indeed guides fibrillarin-induced 2′Ome of mRNAs. Similar to the way microRNAs target mRNAs (36,37), AF357425/SNORD113-6 appears to have many different mRNA targets. However, these targets do appear to be enriched within specific gene pathways, supporting the concept that AF357425/SNORD113-6 plays a specific role in cellular function. Here we focused on the integrin signalling pathway, as it showed the strongest enrichment and as it plays an obvious role in fibroblast function specifically and in cardiovascular disease in general (32). However, we also observed enrichment in various other cardiovascular relevant pathways, including blood coagulation and interleukin signalling. We now looked only at targets affected by the D′ box seed of AF357425/SNORD113-6, but of course both the murine and the human snoRNA have a second seed sequence [which is not fully conserved between species (28)] with its own set of mRNA targets. Furthermore, here we looked at only one of the 34 murine and 41 human DLK1-DIO3 snoRNAs. The total number of mRNAs and gene pathways affected by the DLK1-DIO3 snoRNAs can only be guessed at this stage.

Although the full function of 2′Ome remains to be elucidated, it has been reported that 2′Ome leads to stabilization of the affected RNA molecule (30,31). In fact, synthetic oligonucleotides, including our 3GAs and GMs, are often 2′Ome-modified to increase stability (38). When we inhibited novel transcription by actinomycin D, we indeed observed increased mRNA degradation under snoRNA knockdown. AF357425/SNORD113-6-guided 2′Ome indeed contributes to mRNA stability of its targets. The effects on protein expression, however, were quite ambiguous. Even though *Itgb3* mRNA methylation and expression are reduced and degradation increased under AF357425 inhibition, Itgb3 protein expression is significantly increased in murine cells. A previous study by Elliot *et al*. has shown that 2′Ome of the mRNA can inhibit translation (25); however, the human ITGB3 protein expression was decreased under snoRNA, and thus 2′Ome inhibition, as expected from the mRNA levels. This can be explained by the fact that under SNORD113-6 inhibition, there is a pre-mRNA processing preference for the mRNA variant that is marked for NMD (Ensemble Genome Browser). Clearly, effects of snoRNA binding on protein expression depend on multiple factors, including the location of the binding site (e.g. intron versus 3′UTR) and on whether binding leads to 2′Ome or not. We show here that multiple mechanisms of snoRNA-pre-mRNA interactions and consequences occur simultaneously within the same pathway.

Therefore, more relevant than effects on individual protein expression are effects on cell phenotype as a whole. The DIO3-DLK1 locus is predominantly expressed in fibroblasts (3), and we have also shown previously that DLK1-DIO3 non-coding RNAs are highly relevant to fibroblast phenotype in a cardiovascular setting (11,26,39,40). We show here that the inhibition of SNORD113-6 alters the barrier function of primary human fibroblasts seeded in a monolayer, as well as the ability of fibroblast to contract the extracellular matrix, which are likely the direct consequences of changes in the integrin signalling pathway that plays a crucial role in fibroblast cell–cell and cell–matrix interactions (32). Fibroblast integrin signalling is a crucial pathway in various forms of cardiovascular remodelling that can lead to severe cardiovascular disease (41). Understanding the molecular mechanisms that underlie changes in integrin signalling during the progression of cardiovascular disease may therefore yield novel therapeutic targets.

In conclusion, we show here that DLK1-DIO3 snoRNA AF357425/SNORD113-6 targets a broad range of mRNAs, via two distinct mechanisms, namely pre-mRNA processing/splicing and via 2′Ome, which has a stabilizing effect on mRNA expression. Although AF357425/SNORD113-6 has a broad range of target mRNAs, we do observe clear enrichment of several pathways that play an important role in the progression of cardiovascular disease. AF357425/SNORD113-6 may no longer be a complete ‘orphan’ snoRNA; however, more research into its remaining target RNAs, its second seed sequence and into the other DLK1-DIO3 snoRNAs remains to be done.

Materials and Methods

Cell culture

All cells were cultured in a humidified incubator at 37°C under 5% CO_2. Cells were grown to 70–90% confluency and subsequently passaged. Fresh culture media was added every 2–3 days.

Cell lines

Murine NIH/3T3 embryonic fibroblasts were cultured in DMEM (Invitrogen, GIBCO, Auckland, New Zealand), with 10% heat-inactivated foetal calf serum (FCS; PAA, Pasching, Austria) and 1% penicillin/streptomycin (PenStrep; Lonza, Basel, Switzerland, Cat. Nr. DE17-602E). Human BJ foreskin fibroblasts (ATCC, Manassas, VA, USA) were cultured in MEM (Invitrogen, GIBCO), with 10% heat-inactivated FCS and 1% PenStrep.

Primary murine fibroblasts

PMFs were isolated from ear-clippings of C57BL/6-J mice, ∼3 weeks of age. Ear tissues were cut into smaller pieces and embedded in 0.2% gelatine in 10 cm^2 plates. After embedding, DMEM containing 20% heat-inactivated FCS and 1% non-essential amino acids (NEAA; Gibco, Thermo Fisher, MA, USA, Cat.Nr.11140050) was added and tissues were kept in an incubator at 37°C under 5% CO_2. After ∼7 days, cells were expanded up to passage 3 using culture media (DMEM with 10% heat-inactivated FCS and 1% PenStrep) and frozen down in liquid nitrogen for later use. Cells were used up to passage 5.

Primary human umbilical arterial fibroblasts

Umbilical cords were collected from full-term pregnancies and stored in sterile phosphate buffered saline (PBS) at 4°C and subsequently used for cell isolation within 7 days. The arteries were removed and cleaned from remaining connective tissue. Endothelial cells were removed by gently rolling the artery over a blunted needle. The tunica adventitia and tunica media were separated using surgical forceps. After overnight incubation in HUAF culture medium, (DMEM GlutaMAX™, 10% heat-inactivated FCS, 10% heat-inactivated human serum (PAA), 1% PenStrep and 1% NEAA, the tunica adventitia was incubated in a 2 mg/ml collagenase type II solution (Worthington; OH,

USA, Cat. Nr. NC9693955) at 37°C. Cell suspensions were filtered over a 70 μm cell strainer and centrifuged at 400 g for 10 min. Cell pellets were resuspended and plated in culture medium. To remove slow-adhering non-fibroblast cells, the wells were washed with culture medium after 90 min. HUAFs were then cultured and used up to passage 6.

RNA isolation and RT/qPCR

For RNA isolation, culture media was removed and cells were washed in PBS. After that, cells were lysed with TRIzol (Thermo Fisher, Cat. Nr. 15596026) and RNA was isolated by standard TRIzol-chloroform extraction. RNA concentration and purity were measured using Nanodrop (Nanodrop Technologies, DE, USA) or the Bioanalyzer (2100 Bioanalyzer Instrument, Agilent, CA, USA).

RNA was reverse transcribed using high-capacity RNA-to-cDNA reverse transcription kit (Applied Biosystems, Thermo Fisher, Cat. Nr. 4388950) or the GoScript RT system (Promega) and quantified using Quantitect SybrGreen reagents (Qiagen Benelux, Venlo, The Netherlands, Cat. Nr. 204145) on the VIIa7 (Thermo Fisher, Cat. Nr. 15596026) or using the GoTaq qPCR Master Mix (Promega) on the CFX384 Real-Time System (Bio-Rad). SnoRNA and mRNA expression were normalized to U6 and GAPDH using the $2^{-\Delta Ct}$ method, respectively. All primers used are provided in Supplementary Material, Table S1.

CRISPR/Cas9 of AF357425

We used the commercially available GeneArt CRISPR nuclease vector with OFP reporter (Invitrogen, Thermo Fisher Scientific) to knock out AF357425. When using a single guide RNA did not yield any, surviving, knockout or mutant clones, we used a combination of four guide RNAs, two directed to the positive strand of the AF357425 gene and two directed to the negative strand. Guide RNAs were ordered as two separate DNA oligonucleotides each from Microsynth (Balgach, Switzerland), which were annealed in nuclease-free water using a thermal cycler, starting at 95°C for 5 min, and then decreasing the temperature in 5° steps for 1 min each, until 10°C. The guide RNA sequences were then cloned into the GeneArt CRISPR nuclease vector, according to manufacturer's protocol and clones were checked for inserts using colony PCR. Positive clones were isolated using the PureYield Plasmid Miniprep System (Promega) followed by Sanger Sequencing (Microsynth). For each guide RNA, one clone containing the full and correct sequence was then grown overnight and the vector was purified using the PureYield Plasmid Midiprep System (Promega). Vectors containing the four different guide RNA sequences were then mixed in a 1:1:1:1 ratio. A separate, single, guide RNA was designed and cloned into the GeneArt CRISPR nuclease vector in order to knock out the mutant AF357425 in the BF6 clone. Guide RNA sequences are provided in Supplementary Material, Table S2.

3T3 cells were transfected with the vector mix at a final concentration of 1 μg/μL, using the Calcium Phosphate Transfection Kit (Sigma-Aldrich) according to the manufacturer's protocol. After 24 h, the transfection medium was replaced by conditioned growth medium (medium collected from untransfected 3T3 cells after 24 h of culture) and after another 24 h, cells were trypsinised and replated in 96-well culture plates, using a serial dilution in conditioned medium. Wells containing a single-cell were identified by visual inspection 24–48 h after replating and left to grow into colonies. The presence of mutations in the AF357425 gene was verified using Sanger sequencing and AF357425 expression was checked by RT/qPCR. All primer sequences can be found in Supplementary Material, Table S1.

Analysis of the BF6 clone

In order to obtain the DNA sequences of the heterozygous mutant BF6 clone, primers surrounding the AF357425 gene were used to amplify the BF6 AF357425 genes, which were cloned into the pCR2.1 vector, using the TA cloning kit (Invitrogen by Life Technologies) following the manufacturer's protocol. Clones were checked for inserts using colony PCR. PCR products were separated on a 3% agarose gel, to visualize longer and shorter inserts. One long and one short insert were analysed by Sanger sequencing to obtain sequence information on the two differently mutated alleles.

3rd generation antisense and GMs

3GAs were kindly provided by Idera Pharmaceuticals (Cambridge, MA, USA). 3GAs are made up of two identical strands of DNA-nucleotides with a phosphorothioate backbone, connected by a 5′ phosphorothioate linker. GM consisted of five 2′Ome RNA-nucleotides, 10 DNA-nucleotides and 5 more 2′Ome RNA-nucleotides with full phosphorothioate backbone, and was custom designed and ordered from (Sigma Aldrich, MO, USA, or MicroSynth AG). Sequences of 3GAs and GMs are shown in Supplementary Material, Table S3.

Transfection with 3GAs or GMs

In order to synchronize the cell cycle, cells were treated with KN-93 (Sigma Aldrich, Cat. Nr. K1385), an inhibitor of CaMK-II (the multifunctional Ca2+/CaM kinase), to induce G1 cell cycle arrest (34). KN-93 was added to the culture media (DMEM, 10% FCS and 1% P/S) at a concentration of 10 μM. After 48 h, cells were washed with PBS and DMEM or MEM, depending on the cell type, without serum or PenStrep was added. Lipofectamine RNAiMAX Reagent (Thermo Fisher, Cat. Nr. 13778030) was used to create micelles loaded with 3GAs (200 nM) or GMs (500 nM) against snoRNA AF357425 for transfection. A total of 10% FCS was added to the cells after 1 h of transfection. After 24 h of transfection, cells were washed with PBS and used for further experiments and analyses.

RNA-binding protein immunoprecipitation

RIP was performed using the EZMagna RIP kit (Millipore, Sigma Aldrich, Cat. Nr. 17-701) according to the manufacturer's protocol. All steps were performed on ice and with prechilled buffers. In brief, GM and 3GA transfected PMFs were washed with PBS twice, trypsinised and centrifuged for 5 min at 1500 rpm to form a pellet. Cell pellets were resuspended in 0.1% formaldehyde in order to crosslink the RNA-protein interactions. After crosslinking, cells were centrifuged and pellets were resuspended in complete RIP lysis buffer. Next, cell lysates were incubated with magnetic beads conjugated with antibodies against fibrillarin (Abcam, Cambridge, UK, Cat. Nr. ab5821) or a rabbit control IgG antibody (Millipore, Cat. Nr. PP64B) overnight at 4°C rotating. Prior to incubation with magnetic beads, 10% of the cell lysate was kept separate as an input reference for the immunoprecipitation. Samples with beads were placed in a magnetic separator before aspirating the supernatant. After six washing steps with RIP washing buffer, samples were treated with proteinase K for 30 min at 55°C while shaking. Next, samples were placed in a

magnetic separator and the supernatant was further diluted to a final volume of 250 μL in RNAse free water. RNA was isolated using TRIzol LS Reagent (Thermo Fisher, Cat. Nr. 10296010) for liquid solutions. RNA concentration and purity were measured on the Nanodrop (Nanodrop Technologies) and Bioanalyzer prior to sending them for RNA sequencing (RNA-seq).

RNA-seq and analysis

RNA-seq was outsourced to BGI (Hong Kong). DNBseq Eukaryotic Transcriptome resequencing was performed on the BGISEQ platform with PE100. We performed RNA-seq, both on total RNA isolated from GM versus 3GA transfected PMFs and on the RNA isolated after the fibrillarin RIP. In the latter case, BGI performed an rRNA depletion step before sequencing.

Raw FASTQ files of long RNAseq samples and RIPseq samples were processed using the LUMC BioWDL RNAseq pipeline version 1.1.0 (https://github.com/biowdl/RNA-seq/tree/v1.1.0), which comprises FASTQ preprocessing, alignment and read quantification. Cutadapt (version 2.4) was used for adapters clipping. Reads were further aligned to the mouse reference genome GRCm38 using the STAR aligner (version 2.6.0c). Gene raw read quantification was performed using htseq-count (v0.9.1) with the Ensembl mouse gene annotation version 96. Only uniquely mapped reads are included. In addition, StringTie (v1.3.4) was used to calculate transcripts per million (TPM) of all genes with default settings.

For the long RNA-Seq, BLAST was used to identify 192 genes with a perfect conserved D′ box seed antisense sequence AAACCCCAT in the coding region and 3′UTR. TPM values of these genes, generated from the long RNA-seq, are reported in Supplementary Material, Excel File 1. Genes without variants or genes, which were not expressed in long RNA-seq, were removed from the analysis.

In order to identify all potential targeted mRNAs, we downloaded mouse cDNA sequences from Ensembl FTP and identified all transcripts containing motif sequence AAACCCCAT using a customized Python script. To tolerate binding efficiency, we allowed one base mismatch in the first three bases and last three bases of this motif sequence. By cross-checking these potential binding transcripts with the genes with an increased expression, thus enriched in 3GA (high AF357425) versus GM (low AF357425) in the RIP-Seq samples (fold change expression >1), we identified 407 mouse genes of interest. We converted these murine genes to equivalent human genes, 285 in total (Supplementary Material, Excel File 3). Using the same Python script, we identified 228 out of 285 human genes containing the motif sequence of AAACCCCAT and six of its variants (by allowing one base mismatch in the first three bases and last three bases of this motif sequence). Finally, we performed pathway enrichment analysis on the remaining set of potential target genes using PANTHER Classification System (v.16.0).

The RIP-Seq data were used to identify potential 2′Ome targets of the snoRNA, whereas the normal RNA-Seq was used to compare counts of different transcript variants (as published by Ensembl) within genes, in order to identify changes in mRNA splicing and 3′-end processing.

Detection and estimation of 2′Ome of RNA targets

For the detection of 2′-O-methylated nucleotides, we used an adaptation of the RTL-Q method that was first described by Dong *et al.* (26,42). Briefly, specific RT primers were designed around the site of interest. One forward primer was designed upstream of the possible methylation site (F_U) and one downstream of the methylation site (F_D). One reverse primer (R) was used for both F_U and F_D. The RT reaction was performed in two consecutive steps. First, a mixture of 20 ng RNA and 10 μM reverse primer was denatured at 70°C for 5 min and incubated at 42°C for 10 min as an initial annealing step. Then, a high (200 μM) or low (0,5 μM) concentration of dNTPs (Promega, Cat. Nr. U1511), 200U of M-MLV reverse transcriptase (Promega, Cat. Nr. M1705) and 20U of Recombinant RNasin Ribonuclease Inhibitor (Promega, Cat. Nr. N2515) added to the RT reaction. The RT reaction was incubated at 42°C for 90 min followed by incubation at 75°C for 15 min to deactivate the enzyme. Differences in primer extension efficiency were quantified using SYBR green-based qPCR. To calculate the EMF, we used an adaptation to the method described by Aschenbrenner *et al.* (43).

$$\text{Estimated Methylated fraction} = 1 - E^{-\left(\Delta Ct_{FW-U\ (\text{Low conc.}-\text{High conc.})} - \Delta Ct_{FW-D\ (\text{Low conc.}-\text{High conc.})}\right)}$$

with E = PCR efficiency of FW − D at high dNTP concentration

Detection of processing/splicing variants

Differences in ratios between splice- and 3′-end processing variants of individual putative target genes were quantified using RT/qPCR. Where possible, we used the same forward primer, with a variable reverse primer in order to pick up the different variants. All primers are provided in Supplementary Material, Table S1. We used Ensemble Genome Browser to look up transcript variants in the human genome (GRCh38.p13) and murine genome (GRCm39). Variants with or without AF357425/SNORD113-6 binding site were named variant 1 or variant 2, respectively (Supplementary Material, Fig. S2). Only relevant transcripts either with or without binding sites are shown. Ratio was calculated as variant 2 divided by variant 1. Of note, the product variant 2 is the sum of variant 1 and 2, as primers designed for variant 2 target exons/introns present in both variants, except for human *MAP2K1*, *DUSP7* and *EBPL* and murine *Dusp7*, for which both variants were measured with fully separate primer sets (Supplementary Material, Table S1).

Western blotting

Cells were washed with PBS and lysed using liquid nitrogen. Proteins were denatured using Laemmli buffer (2× buffer: 0.125 M Tris base, 4% SDS, 20% glycerol, 10% beta-mercaptoethanol, 2 mg bromophenol blue per ml buffer, pH ∼6.8) and loaded onto Mini-PROTEAN® TGX™ Precast Protein gels (10–15%, Bio-Rad). After separation, proteins were transferred onto polyvinylidene difluoride membranes (0.45 μm, Carl Roth). Membranes were blocked in 5% Non-Fat Milk buffer (Bio-Rad) for 1 h at room temperature and probed with the primary antibodies overnight at 4°C. The following primary antibodies were used:), rabbit polyclonal anti-MEK-1 [(MAP2K1) 1:1000, PA5-16556, Invitrogen, Thermo Fisher Scientific], rabbit polyclonal anti-CD61 [(ITGB3) 1:1000, PA5-85926, Invitrogen, Thermo Fisher Scientific], rabbit polyclonal anti-JAG1 (1:1000, PA5-72843, Invitrogen, Thermo Fisher Scientific), rabbit polyclonal anti-DUSP7 (1:1000,PA5-100490, Invitrogen, Thermo Fisher Scientific) and rabbit polyclonal anti-GAPDH (1:10.000-20.000, PA1-987, Invitrogen, Thermo Fisher Scientific). Membranes were washed with 0.1% Tween 20 PBS and probed with the secondary HRP-conjugated anti-rabbit IgG antibody (1:2500–5000) at room temperature for 2 h. Protein levels were detected using chemiluminescence by SuperSignal West Femto Maximum Sensity Substrate (Invitrogen, Thermo Fisher Scientific). Intensities of the obtained signals were normalized to the intensities of the GAPDH control bands.

mRNA stability

In order to measure effects on mRNA stability, HUAFs and PMFs were treated with 10 μM KN-93 for 48 h and subsequently transfected with GMs against SNORD-113-6 or AF357425, respectively, or a negative control, as described earlier. After 24 h, cells were treated with 5 $\mu g/\mu l$ Actinomycin D (Sigma Aldrich, Cat. Nr. A9415), to inhibit novel RNA transcription. We then measured mRNA expression at 2 (T2) and 6 (T6) hours after addition of Actinomycin D and calculated the decline in mRNA over time (T6-T2).

Fibroblast barrier function

Electric cell-substrate impedance sensing (Model 1600R, Applied Biophysics, NY, USA) is a method to quantify cell function over time. Cells are seeded on an electrode and impedance is then used as a measure of electrode coverage, cell number and cell attachment (44). For this assay, 8 well/10 electrode plates were used (Ibidi, Gräfelfing, Germany, Cat. Nr. 72010). Prior to seeding cells, electrodes were coated with 10 nM l-cysteine (Sigma, Steinheim, Germany, 30 089-25G) and 1% gelatine (Merck, Darmstadt, Germany, 1 040 700 500). Fibroblasts were collected 24 h after KN-93 treatment and GM transfection and seeded at a density of 50.000 cells per well in DMEM (+10% FCS and 1% PenStrep). Impedance was measured over time at multiple frequencies 62–64 000 Hz).

Collagen gel contraction

Extracellular matrix contraction was simulated by embedding fibroblasts in a collagen lattice gel as described by Ngo *et al.* (45). GM-transfected HUAFs were suspended in a 2 mg/mL collagen type I (Millipore, Sigma Aldrich, Cat. Nr. 08-115) solution at a concentration of 1.5×10^5 cells/mL, together with 10 μM KN-93. We then poured 350 μL collagen gels in a 48-well plate and allowed the gels to solidify for 20 min at room temperature. Gels were dissociated from the mould and resuspended in DMEM (+10% FCS and 1% PenStrep). Pictures were taken at 0 (T0), 24 (T24) and 48 h (T48) after dissociation, and contraction was analysed using ImageJ software (National Institutes of Health, Bethesda, MD, USA, https://imagej.nih.gov/ij/, 1997–2018).

Scratch wound healing assay

In order to investigate cell migration, HUAFs were treated with 10 μM KN-93 for 48 h and subsequently transfected with GMs against SNORD-113-6 or a negative control, as described earlier. A total of 24 h after transfection, a scratch was introduced by scraping a straight line using a p200 pipet tip in the cell monolayer. Cells were washed with PBS to remove any debris. Cells were incubated for 24 h in culture medium containing 10 μM KN-93 to inhibit cell proliferation. Pictures were taken under a phase-contrast microscope at 0 (T0) and 24 (T24) hours after introducing the scratch. Cell migration was analysed using ImageJ software (National Institutes of Health, https://imagej.nih.gov/ij/, 1997–2018).

Statistical analyses

Results are expressed as mean ± standard error of mean (SEM). As knockdown efficiency varied per experiment, we performed paired *t*-tests to compare each treatment with its own control, within each individual experiment. GraphPad (v.8.4.2) was used to perform all statistical analyses. $P < 0.05$ was considered significant and $P < 0.1$ was considered a trend.

Supplementary Material

Supplementary Material is available at *HMG* online.

Data availability

All data are available in the main manuscript or in the Supplementary Material. RNA-Seq data are also available in the Gene Expression Omnibus under accession number GSE173099.

Acknowledgements

We kindly acknowledge Neda Ektefaie, Bart Boersma, Martijn Willemsen and Pleun Engbers for their technical support.

Conflict of Interest statement. None declared.

Funding

Rembrandt Institute of Cardiovascular Science (A.Y.N, R.A.B); Austrian Science Fund FWF (M2578-B30 to A.Y.N.).

Author contributions

E.v.I., D.A.L.v.d.H., V.K. and N.P.M. performed experiments, M.L.v.d.B. and H.M .performed RNA-Seq data analyses, R.A.B. and A.Y.N. designed experiments, E.v.I., D.A.L.v.d.H. and A.Y.N. wrote the manuscript, R.A.B., P.H.A.Q. and J.W. critically reviewed the manuscript, R.A.B. and A.Y.N. acquired funding.

References

1. Kiss, T. (2001) Small nucleolar RNA-guided post-transcriptional modification of cellular RNAs. *EMBO J.*, **20**, 3617–3622.
2. Monaco, P.L., Marcel, V., Diaz, J.J. and Catez, F. (2018) 2'-O-methylation of ribosomal RNA: towards an epitranscriptomic control of translation? *Biomol. Ther.*, **8**, 106.
3. Jorjani, H., Kehr, S., Jedlinski, D.J., Gumienny, R., Hertel, J., Stadler, P.F., Zavolan, M. and Gruber, A.R. (2016) An updated human snoRNAome. *Nucleic Acids Res.*, **44**, 5068–5082.
4. Falaleeva, M., Welden, J.R., Duncan, M.J. and Stamm, S. (2017) C/D-box snoRNAs form methylating and non-methylating ribonucleoprotein complexes: old dogs show new tricks. *BioEssays*, **39**, 1600264.
5. Hakansson, K.E.J., Goossens, E.A.C., Trompet, S., van Ingen, E., de Vries, M.R., van der Kwast, R., Ripa, R.S., Kastrup, J., Hohensinner, P.J., Kaun, C. *et al.* (2019) Genetic associations and regulation of expression indicate an independent role for 14q32 snoRNAs in human cardiovascular disease. *Cardiovasc. Res.*, **115**, 1519–1532.
6. Lin, S.P., Youngson, N., Takada, S., Seitz, H., Reik, W., Paulsen, M., Cavaille, J. and Ferguson-Smith, A.C. (2003) Asymmetric regulation of imprinting on the maternal and paternal chromosomes at the Dlk1-Gtl2 imprinted cluster on mouse chromosome 12. *Nat. Genet.*, **35**, 97–102.
7. Boon, R.A., Hofmann, P., Michalik, K.M., Lozano-Vidal, N., Berghauser, D., Fischer, A., Knau, A., Jae, N., Schurmann, C. and Dimmeler, S. (2016) Long noncoding RNA Meg3 controls endothelial cell aging and function: implications for regenerative angiogenesis. *J. Am. Coll. Cardiol.*, **68**, 2589–2591.

8. Michalik, K.M., You, X., Manavski, Y., Doddaballapur, A., Zornig, M., Braun, T., John, D., Ponomareva, Y., Chen, W., Uchida, S. *et al.* (2014) Long noncoding RNA MALAT1 regulates endothelial cell function and vessel growth. *Circ. Res.*, **114**, 1389–1397.
9. Nossent, A.Y., Eskildsen, T.V., Andersen, L.B., Bie, P., Bronnum, H., Schneider, M., Andersen, D.C., Welten, S.M., Jeppesen, P.L., Hamming, J.F. *et al.* (2013) The 14q32 microRNA-487b targets the antiapoptotic insulin receptor substrate 1 in hypertension-induced remodeling of the aorta. *Ann. Surg.*, **258**, 743–751 discussion 752-743.
10. van Ingen, E., Foks, A.C., Kroner, M.J., Kuiper, J., Quax, P.H.A., Bot, I. and Nossent, A.Y. (2019) Antisense oligonucleotide inhibition of MicroRNA-494 halts atherosclerotic plaque progression and promotes plaque stabilization. *Mol Ther Nucleic Acids*, **18**, 638–649.
11. Welten, S.M., Bastiaansen, A.J., de Jong, R.C., de Vries, M.R., Peters, E.A., Boonstra, M.C., Sheikh, S.P., La Monica, N., Kandimalla, E.R., Quax, P.H. *et al.* (2014) Inhibition of 14q32 MicroRNAs miR-329, miR-487b, miR-494, and miR-495 increases neovascularization and blood flow recovery after ischemia. *Circ. Res.*, **115**, 696–708.
12. Welten, S.M., Goossens, E.A., Quax, P.H. and Nossent, A.Y. (2016) The multifactorial nature of microRNAs in vascular remodelling. *Cardiovasc. Res.*, **110**, 6–22.
13. Welten, S.M.J., de Jong, R.C.M., Wezel, A., de Vries, M.R., Boonstra, M.C., Parma, L., Jukema, J.W., van der Sluis, T.C., Arens, R., Bot, I. *et al.* (2017) Inhibition of 14q32 microRNA miR-495 reduces lesion formation, intimal hyperplasia and plasma cholesterol levels in experimental restenosis. *Atherosclerosis*, **261**, 26–36.
14. Welten, S.M.J., de Vries, M.R., Peters, E.A.B., Agrawal, S., Quax, P.H.A. and Nossent, A.Y. (2017) Inhibition of Mef2a enhances neovascularization via post-transcriptional regulation of 14q32 MicroRNAs miR-329 and miR-494. *Mol Ther Nucleic Acids*, **7**, 61–70.
15. Wezel, A., Welten, S.M., Razawy, W., Lagraauw, H.M., de Vries, M.R., Goossens, E.A., Boonstra, M.C., Hamming, J.F., Kandimalla, E.R., Kuiper, J. *et al.* (2015) Inhibition of MicroRNA-494 reduces carotid artery atherosclerotic lesion development and increases plaque stability. *Ann. Surg.*, **262**, 841–847 discussion 847–848.
16. Cavaille, J., Seitz, H., Paulsen, M., Ferguson-Smith, A.C. and Bachellerie, J.P. (2002) Identification of tandemly-repeated C/D snoRNA genes at the imprinted human 14q32 domain reminiscent of those at the Prader-Willi/Angelman syndrome region. *Hum. Mol. Genet.*, **11**, 1527–1538.
17. Cavaille, J., Buiting, K., Kiefmann, M., Lalande, M., Brannan, C.I., Horsthemke, B., Bachellerie, J.P., Brosius, J. and Huttenhofer, A. (2000) Identification of brain-specific and imprinted small nucleolar RNA genes exhibiting an unusual genomic organization. *Proc. Natl. Acad. Sci. U. S. A.*, **97**, 14311–14316.
18. Bortolin-Cavaillé, M.L. and Cavaillé, J. (2012) The SNORD115 (H/MBII-52) and SNORD116 (H/MBII-85) gene clusters at the imprinted Prader-Willi locus generate canonical box C/D snoRNAs. *Nucleic Acids Res.*, **40**, 6800–6807.
19. Prasasya, R., Grotheer, K.V., Siracusa, L.D. and Bartolomei, M.S. (2020) Temple syndrome and Kagami-Ogata syndrome: clinical presentations, genotypes, models and mechanisms. *Hum. Mol. Genet.*, **29**, R107–R116.
20. Kishore, S., Khanna, A., Zhang, Z., Hui, J., Balwierz, P.J., Stefan, M., Beach, C., Nicholls, R.D., Zavolan, M. and Stamm, S. (2010) The snoRNA MBII-52 (SNORD 115) is processed into smaller RNAs and regulates alternative splicing. *Hum. Mol. Genet.*, **19**, 1153–1164.
21. Kishore, S. and Stamm, S. (2006) Regulation of alternative splicing by snoRNAs. *Cold Spring Harb. Symp. Quant. Biol.*, **71**, 329–334.
22. Kishore, S. and Stamm, S. (2006) The snoRNA HBII-52 regulates alternative splicing of the serotonin receptor 2C. *Science*, **311**, 230–232.
23. Falaleeva, M., Pages, A., Matuszek, Z., Hidmi, S., Agranat-Tamir, L., Korotkov, K., Nevo, Y., Eyras, E., Sperling, R. and Stamm, S. (2016) Dual function of C/D box small nucleolar RNAs in rRNA modification and alternative pre-mRNA splicing. *Proc. Natl. Acad. Sci. U. S. A.*, **113**, E1625–E1634.
24. Huang, C., Shi, J., Guo, Y., Huang, W., Huang, S., Ming, S., Wu, X., Zhang, R., Ding, J., Zhao, W. *et al.* (2017) A snoRNA modulates mRNA 3′ end processing and regulates the expression of a subset of mRNAs. *Nucleic Acids Res.*, **45**, 8647–8660.
25. Elliott, B.A., Ho, H.T., Ranganathan, S.V., Vangaveti, S., Ilkayeva, O., Abou Assi, H., Choi, A.K., Agris, P.F. and Holley, C.L. (2019) Modification of messenger RNA by 2'-O-methylation regulates gene expression in vivo. *Nat. Commun.*, **10**, 3401.
26. van der Kwast, R., van Ingen, E., Parma, L., Peters, H.A.B., Quax, P.H.A. and Nossent, A.Y. (2018) Adenosine-to-inosine editing of MicroRNA-487b alters target gene selection after ischemia and promotes neovascularization. *Circ. Res.*, **122**, 444–456.
27. Brameier, M., Herwig, A., Reinhardt, R., Walter, L. and Gruber, J. (2011) Human box C/D snoRNAs with miRNA like functions: expanding the range of regulatory RNAs. *Nucleic Acids Res.*, **39**, 675–686.
28. Hakansson, K.E.J., Sollie, O., Simons, K.H., Quax, P.H.A., Jensen, J. and Nossent, A.Y. (2018) Circulating small noncoding RNAs as biomarkers for recovery after exhaustive or repetitive exercise. *Front. Physiol.*, **9**, 1136.
29. Ploner, A., Ploner, C., Lukasser, M., Niederegger, H. and Huttenhofer, A. (2009) Methodological obstacles in knocking down small noncoding RNAs. *RNA*, **15**, 1797–1804.
30. Ji, L. and Chen, X. (2012) Regulation of small RNA stability: methylation and beyond. *Cell Res.*, **22**, 624–636.
31. Motorin, Y. and Helm, M. (2010) tRNA stabilization by modified nucleotides. *Biochemistry*, **49**, 4934–4944.
32. Jang, Y., Lincoff, A.M., Plow, E.F. and Topol, E.J. (1994) Cell adhesion molecules in coronary artery disease. *J. Am. Coll. Cardiol.*, **24**, 1591–1601.
33. Filippova, J.A., Matveeva, A.M., Zhuravlev, E.S., Balakhonova, E.A., Prokhorova, D.V., Malanin, S.J., Shah Mahmud, R., Grigoryeva, T.V., Anufrieva, K.S., Semenov, D.V. *et al.* (2019) Are small nucleolar RNAs "CRISPRable"? A report on box C/D small nucleolar RNA editing in human cells. *Front. Pharmacol.*, **10**, 1246.
34. Tombes, R.M., Grant, S., Westin, E.H. and Krystal, G. (1995) G1 cell cycle arrest and apoptosis are induced in NIH 3T3 cells by KN-93, an inhibitor of CaMK-II (the multifunctional Ca2+/CaM kinase). *Cell Growth Differ.*, **6**, 1063–1070.
35. Downie Ruiz Velasco, A., Welten, S.M.J., Goossens, E.A.C., Quax, P.H.A., Rappsilber, J., Michlewski, G. and Nossent, A.Y. (2019) Posttranscriptional regulation of 14q32 MicroRNAs by the CIRBP and HADHB during vascular regeneration after ischemia. *Mol Ther Nucleic acids*, **14**, 329–338.
36. Bartel, D.P. (2004) MicroRNAs: genomics, biogenesis, mechanism, and function. *Cell*, **116**, 281–297.

37. van Rooij, E. and Olson, E.N. (2012) MicroRNA therapeutics for cardiovascular disease: opportunities and obstacles. *Nat. Rev. Drug Discov.*, **11**, 860–872.
38. Yu, D., Iyer, R.P., Shaw, D.R., Lisziewicz, J., Li, Y., Jiang, Z., Roskey, A. and Agrawal, S. (1996) Hybrid oligonucleotides: synthesis, biophysical properties, stability studies, and biological activity. *Bioorg. Med. Chem.*, **4**, 1685–1692.
39. van der Kwast, R., Parma, L., van der Bent, M.L., van Ingen, E., Baganha, F., Peters, H.A.B., Goossens, E.A.C., Simons, K.H., Palmen, M., de Vries, M.R. *et al.* (2020) Adenosine-to-inosine editing of vasoactive MicroRNAs alters their targetome and function in ischemia. *Mol Ther Nucleic Acids*, **21**, 932–953.
40. van der Kwast, R., Quax, P.H.A. and Nossent, A.Y. (2019) An emerging role for isomiRs and the microRNA epitranscriptome in neovascularization. *Cell*, **9**, 61.
41. Civitarese, R.A., Kapus, A., McCulloch, C.A. and Connelly, K.A. (2017) Role of integrins in mediating cardiac fibroblast-cardiomyocyte cross talk: a dynamic relationship in cardiac biology and pathophysiology. *Basic Res. Cardiol.*, **112**, 6.
42. Dong, Z.W., Shao, P., Diao, L.T., Zhou, H., Yu, C.H. and Qu, L.H. (2012) RTL-P: a sensitive approach for detecting sites of 2'-O-methylation in RNA molecules. *Nucleic Acids Res.*, **40**, e157.
43. Aschenbrenner, J. and Marx, A. (2016) Direct and site-specific quantification of RNA 2'-O-methylation by PCR with an engineered DNA polymerase. *Nucleic Acids Res.*, **44**, 3495–3502.
44. Szulcek, R., Bogaard, H.J. and van Nieuw Amerongen, G.P. (2014) Electric cell-substrate impedance sensing for the quantification of endothelial proliferation, barrier function, and motility. *J. Vis. Exp.*, **85**, e51300.
45. Ngo, P., Ramalingam, P., Phillips, J.A. and Furuta, G.T. (2006) Collagen gel contraction assay. *Methods Mol. Biol.*, **341**, 103–109.